Geomorphic evidence for recent uplift of the Fitzcarrald Arch (Peru): a response to the Nazca Ridge subduction

Vincent Regard, Renaud Lagnous, Nicolas Espurt, Patrice Baby, José Darrozes, Martin Roddaz, Ysabel Calderon, Wilber Hermoza

Geomorphic evidence for recent uplift of the Fitzcarrald Arch (Peru): a response to the Nazca Ridge subduction

V. Regard[1], R. Lagnous[1], N. Espurt[1,*], J. Darrozes[1], P. Baby[1,2,3], M. Roddaz[1], Y. Calderon[3] & W. Hermoza[3,$]

1- Université de Toulouse; UPS (SVT-OMP); LMTG; 14 Av, Edouard Belin, F-31400 Toulouse, France
2- IRD; LMTG; F-31400 Toulouse, France
3- PerùPetro SA, Lima, Peru
* Now at CEREGE-CNRS-Université Aix-Marseille III, Plateau de l'Arbois, BP80, F-13545 Aix-en-Provence, France
$ Now at REPSOL-YPF, Paseo de la Castellana 280, 1ª Pl., 28046 Madrid, Spain

Abstract

The 400 000 km^2-wide Fitzcarrald Arch constitutes a wide topographic high of the Amazon Basin against the central Andes. In order to constrain its formation mechanisms and in particular to test its relationships to the Nazca ridge subduction, a quantitative geomorphology analysis of the Arch is performed using hypsometric integrals, elongation and azimuths of 7th- and 5th-order catchments. They all express a trend from high maturity to low maturity from NW towards SE. This maturity gradient coupled with the local drainage direction demonstrate that the Fitzcarrald Arch is not a 'classical' alluvial fan, since its apex is located 100 km east to the Subandean Thrust Front and the corresponding sedimentary pile is lacking. Nor it the Arch the superficial expression of an inherited transfer zone, because its geomorphic shape is radial and it does not diverge from a symmetry axis; moreover, such a reactivated structure is not found at depth on seismic profiles. In addition, our data show that underlying geomorphic control on catchment initiation and development has progressed from NW to SE, which in combination with the observation of crustal doming by Espurt et al. (2007) suggests that this relief is caused by the eastward sliding of the buoyant Nazca ridge beneath the South American lithosphere.

Keywords: Geomorphology; Hypsometry; Elongation; Ridge subduction; Nazca Ridge; Andes; Amazonian basin; Peru; Foreland; Forebulge.

1 Introduction

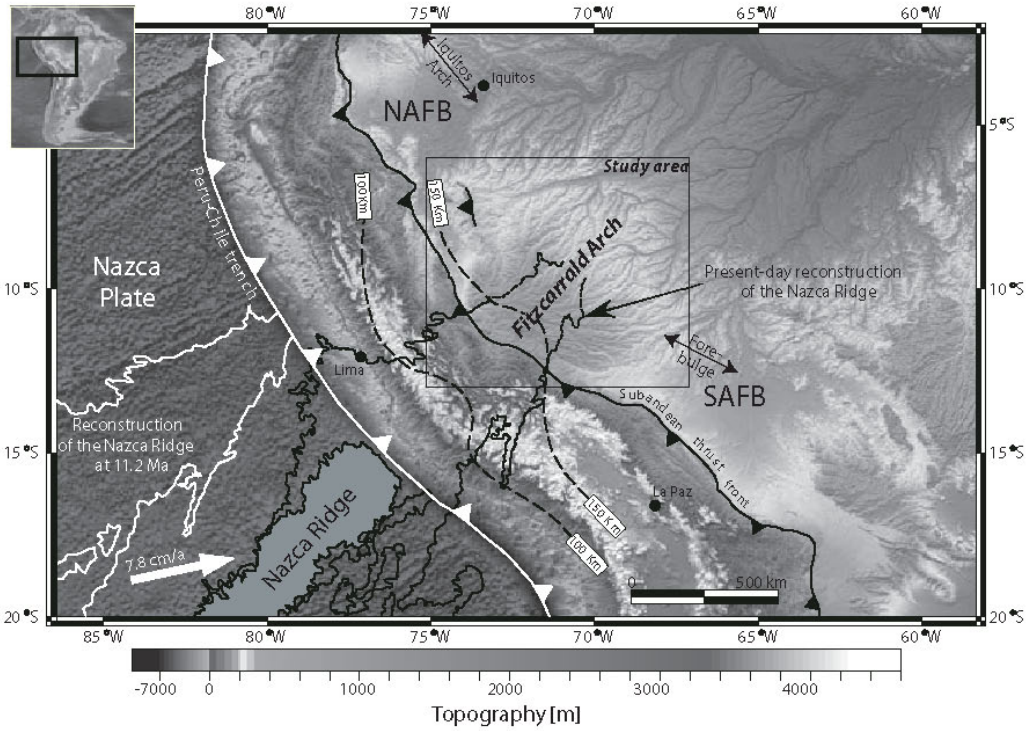

Figure 1. *Geodynamic setting of the Peruvian Andes and its associated Amazonian foreland basin (taken from Espurt et al., 2007). The flat slab segment is illustrated by isodepth contours of Wadati-Benioff zone (Gutscher et al., 1999), and plate convergence vector is from NUVEL1A plate kinematics model (DeMets et al., 1990). NAFB: northern Amazonian foreland basin; SAFB: southern Amazonian foreland basin Black line: present-day reconstruction of the subducted part of the Nazca Ridge (Hampel, 2002). The ridge reconstruction at 11.2 Ma is shown (white line, Hampel, 2002). The easternmost edge of the Nazca Ridge is not involved in the flat slab; it is brought by the sinking slab: its projection at surface may differ from the reconstruction represented by the dotted line. The rectangle indicates the study area covered by next figures. The forebulge is located after the works of Aalto et al. (2003) in the SAFB and Roddaz et al. (2005a) as the Iquitos Arch in the NAFB.*

Ridge subduction is currently actively debated in terms of geodynamics and superficial tectonics above the subduction zone. In the recent past, the western South American margin was regarded as a key place to investigate the effect of ridge subduction on

upper plate tectonics (Gutscher, 2002; Hampel, 2002; Yañez et al., 2002; Espurt et al., 2008b). Indeed, contrary to a "normal subduction" characterized by a gently dipping subducting plate, superficial seismic activity concentrated at the subduction zone and some volcanic activity, ridge subduction can result in "flat subduction" zones where the subduction plane flattens at ~100 km depth under the continental plate, volcanic activity disappears and some seismic activity appears in a back-arc position (Gutscher, 2002; Espurt et al., 2008b), like in the Sierras Pampeanas in Argentina (Jordan et al., 1983).

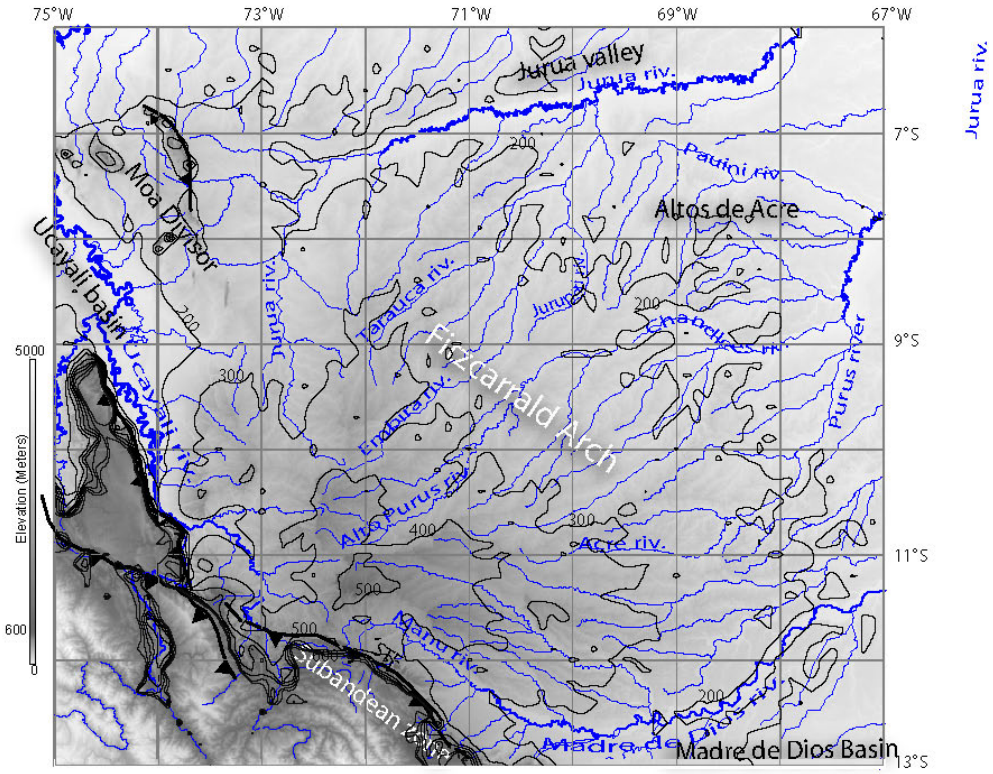

Figure 2. *Shuttle Radar Topography Mission (SRTM) Digital Elevation Model (DEM) of the Fitzcarrald Arch, with main rivers and smoothed elevation contours between 100 and 1000 masl. The Fitzcarrald Arch develops east of the Subandean Thrust Front (STF) and south of the Moa Divisor range, where some young thrusts are cutting through the cover. A-A' and B-B' are the topographic cross-section locations (Fig. 4) and C-C' is the seismic section (Fig. 5).*

The Fitzcarrald Arch constitutes a major geomorphic feature spreading more than 400 000 km^2 in the Amazon basin, extending from southern Peru to western Brazil (Fig. 1) (Church, 1901; Espurt et al., 2007). It lies east of the Subandean Thrust Front and south of the

65 Moa Divisor Range (Latrubesse and Rancy, 2000), where no thrust deformation occurs; the
66 Arch separates the foredeeps of the northern and southern Amazonian foreland basins (Fig. 1)
67 (Hermoza et al., 2005; Roddaz et al., 2005a). To the east it is bounded by the subsiding
68 eastern Amazon basin (Kronberg et al., 1998). This 400 to 600 m-elevated relief dominates
69 the foreland basins lying at ~120 m asl (meters above sea level) and ~150 m asl, and behaves
70 as an ecological boundary with different genetic evolution to the north than to the south (Daly
71 and Mitchell, 2000).

72 The arch has a dome-like morphology with radial drainage network, originating at a
73 point close to main Andean river catchment outlets, i.e., at the break in slope separating the
74 steep Andean slope from the very gentle slopes of the Amazon Basin, which argues for simple
75 mega-fan geometry (Figs. 2, 3). The fan sediment would have been supplied by the Andean
76 tributaries of the Ucayali (flowing northward towards Marañon and Amazon rivers) and
77 Madre de Dios rivers (flowing eastward towards Beni River in Bolivia) (Fig. 2). In addition,
78 these observations are strongly supported by the Pliocene and Pleistocene fluvial deposits that
79 cover the Fitzcarrald Arch (Espurt et al., 2007). Megafans are found elsewhere near the
80 Subandean zone, for example in Ecuador (Christophoul et al., 2002). In particular, in Bolivia,
81 modern and ancient megafans led Horton and DeCelles (2001) to the conclusions that they are
82 deposited through frequent avulsions, reaching sizes of about 10^4 km^2. One implication
83 important for the present work is that the top surface of a megafan is quasi-isochronous; hence
84 all the catchments over the megafan surface must develop at the same time after the end of
85 megafan building. In the study of Horton and DeCelles (2001) the megafan corresponding to
86 the Camargo formation is about 2 km thick.

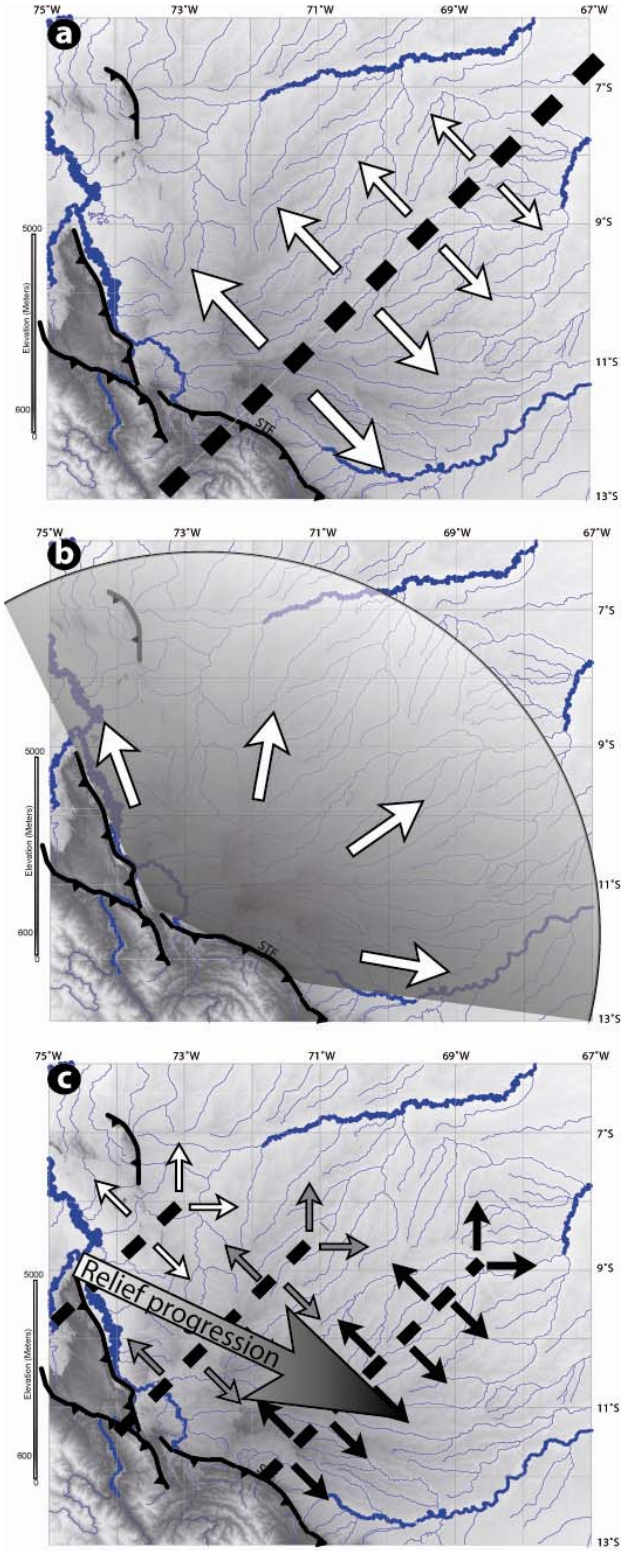

Figure 3. *The three scenarios explored in the paper. The arrows indicate the river network expected trends. (a) Transfer zone scenario. The transfer zone is thought to trend ~N45°E; the relief is developing away from the axis of the transfer zone (black discontinuous line). (b) The fan scenario. The rivers may radiate from the fan apex located near the Subandean Thrust Front. (c) The Nazca Ridge subduction scenario. The river network diverges from the Nazca ridge axis (black discontinuous line), but its location and consequent river network development progresses from north-west to south-east (indicated by colour variation from white to black).*

Recently, some authors have proposed alternative hypotheses for the Fitzcarrald Arch formation. Analysis of Subandean basin geometries and subsidence histories all over South America leads Jacques (2003) to the conclusion that the Subandean basins behave more or less independently. These basins would have been separated by lithospheric fault zones (transfer zones), probably inherited from old structures affecting the overall lithosphere, and crossing the entire South America continent (Jacques, 2003; Carlotto et al., 2007). The transfer zones would correspond to ancient strike slip fault zones and are divided into two groups whose respective orientations are NW-SE and ENE-WSW. The Fitzcarrald Arch would then be the surface expression of one of these transfer zones: the ENE-trending Pisco–Abancay–Fitzcarrald lineament (Jacques, 2003) (Fig. 3).

Another hypothesis comes from geodynamics. Currently, the Nazca plate (Fig. 1) is subducting underneath South America at a velocity of 7.7 cm/yr in a direction N78°E at 15°S (DeMets et al., 1990) (Fig. 1). It brings an oceanic ridge, the 1500m-high, up to 200 km-wide Nazca ridge (Woods and Okal, 1994), whose buoyancy is thought to be the cause of the flat slab subduction beneath central Peru (Gutscher et al., 2000). At surface, flat slab subduction is usually characterized by a lack of active volcanism and by active, distributed deformation of the overriding plate far from the trench, up to several hundreds of kilometres in land (Gutscher et al., 2000; Gutscher, 2002). The ridge must have originated at the Pacific-Nazca spreading centre, allowing Hampel (2002) to reconstruct the shape and position of the subducted part of the ridge on the basis of its remaining symmetrical part on the Pacific Plate, which is the Tuamotu plateau (Fig. 1). Interestingly, the ridge is N42°E-trending, oblique with respect to the plate convergence. It results in a south-eastward migration of the ridge subduction point along the Peruvian coast. The ridge first entered the trench ~11.2 Ma ago at 11°S; this entrance point is now located at 15°S (Hampel, 2002) (Fig. 1). These results led Dumont (1996) to hypothesize a link between flat subduction and the Fitzcarrald Arch. Espurt

et al. (2007), using morphologic evidence and subsurface data coupled with Hampel's (2002) reconstruction, show that the flat subduction zone as well as the Nazca ridge reconstruction fully coincide with the Fitzcarrald Arch location (Fig. 1). The Nazca Ridge probably reached the area under the Fitzcarrald Arch at around 4 Ma. Espurt et al. (2007) seismic profile observations indicate that the overall sedimentary pile has a dome-shape, likely caused by deep processes, i.e., by the buoyant Nazca Ridge subduction.

To distinguish between these hypotheses about the formation of the Fitzcarrald Arch, our study aims to use quantitative geomorphology, by applying multiple indicators of catchment maturity, such as hypsometry or catchment shape (Fig. 3).

2 Geological and geomorphological setting

The Fitzcarrald Arch is characterized by a radial, but asymetrical, drainage network (Fig. 2), leading to the three Amazonian basins indicated above. It has an asymmetrical shape; its south eastern flank dips gently at 0.1° whereas its northwestern slope is hillier and its dip reaches 0.3° (Fig. 4). From the Subandean Thrust Front to the Amazon basin, in a SW-NE direction its dip progressively falls from 0.12° to 0.02° (Fig. 4 and Espurt et al., submitted).

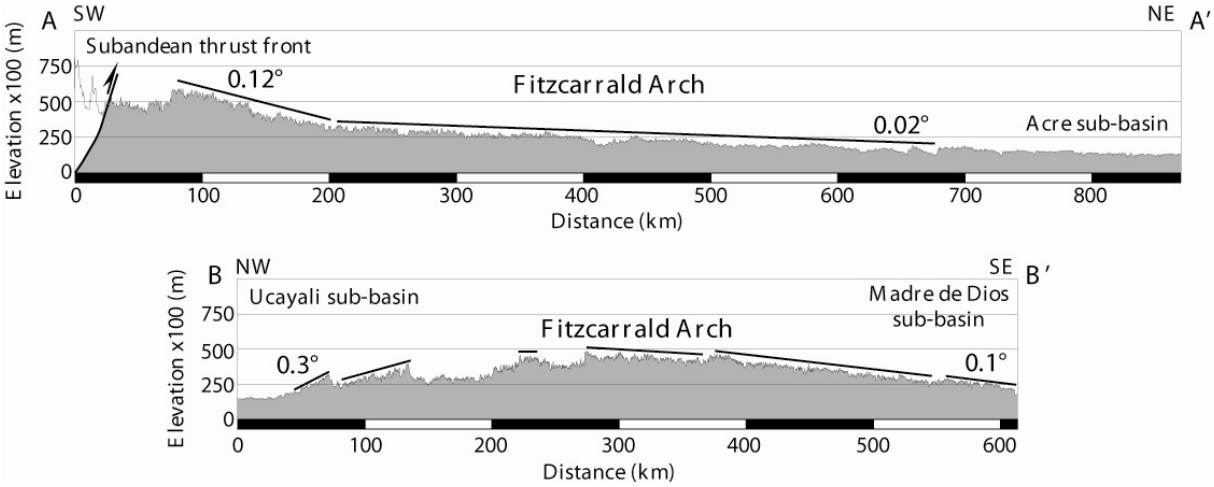

Figure 4. *Topographic profiles of the Fitzcarrald Arch, perpendicular (A-A') and parallel (B-B') to the Subandean Thrust Front (see Fig. 2 for location). The regional slopes are indicated.*

The Arch is constituted at depth by a discontinuous sedimentary sequence from early Palaeozoic to Pleistocene age. Seismic reflection profiles indicate many pre-Cretaceous tectonic structures sealed by Cretaceous strata. Neogene strata overlie Cretaceous deposits and are currently exposed and eroded. The outcrops are organised from older in the north-western centre of the Arch to younger at the edges of the Arch (Espurt et al., submitted). The oldest formations outcropping are middle to late Miocene sediments indicating fluvial to tide-influenced environments, as described in several parts of the Amazonian foreland basin (Räsänen et al., 1995; Gingras et al., 2002; Hovikoski et al., 2005; Rebata et al., 2006; Roddaz et al., 2006; Hovikoski et al., 2007; e.g., Espurt et al., submitted). These tidal deposits show that this part of the Amazonian foreland basin was a subsiding foredeep during the late Miocene. On the contrary, Pliocene to recent deposits consist of coarse-grained fluvial deposits, indicating a change in the geodynamic context of the Amazon Basin from an underfilled to an overfilled basin during the late Miocene or early Pliocene. On the basis of wells and vitrinite reflectance (reflecting the thermal history), Espurt (2007) inferred a total erosion of the order of 500-700 m since the beginning of Pliocene in the north-western central part of the Arch. Consequently, the upper bound for the fluvial catchments' initiation and development corresponds to the emersion of the system around late Miocene/early Pliocene. Unfortunately, even if tidal deposits are found all around the Arch edges, it is not possible to detect differences in the timing of submersion due to a lack of accuracy of chronological constraints.

In addition, seismic reflection profiles across the Arch show that sediment beddings are roughly parallel the overall topography, in a wide dome structure, whose north-western and south-eastern flanks dip 0.3° and 0.1°, respectively (Fig. 5) (Espurt et al., 2007). In particular, Miocene sediments show no significant thickness variation that precludes a synsedimentary Miocene uplift (Espurt, 2007). Seismic reflection profiles indicate no

significant Neogene faulting in the study area with the exception of the Subandean Thrust Front, and the Moa Divisor area where some reactivation of Palaeozoic structures can be found (Hermoza et al., 2005; Espurt et al., 2008a).

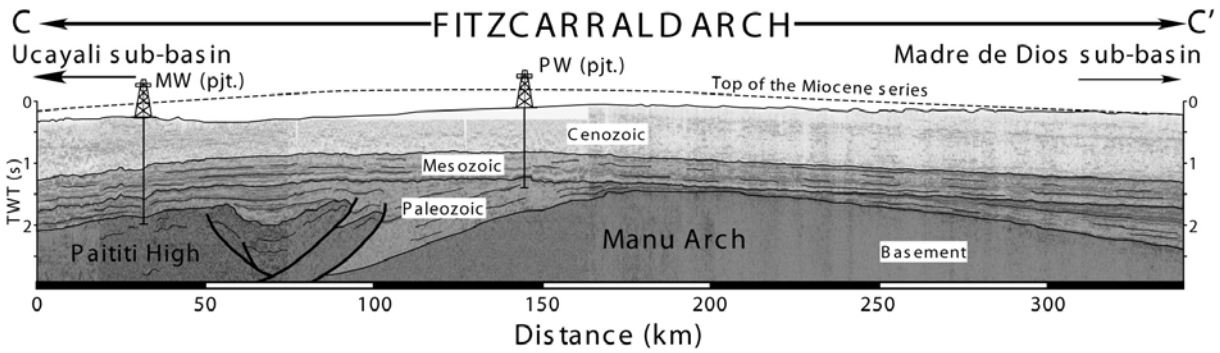

Figure 5. *Interpreted regional seismic reflection profile of the Fitzcarrald Arch and 2 control wells (see location in Fig. 2). No tectonic structure younger than Paleozoic times can be seen, just a regional uplift of the sedimentary strata more than 700 m in the central part of the Arch.*

Another important geological feature of the Amazon Basin is the presence of the forebulge. It corresponds to an elastic rebound due to the elastic flexure of the Andes over the South America plate. It must be responsible for vertical displacements up to 100 meters. It has been invoked for the Iquitos Arch north of our study area, on the basis of sedimentation history, geomorphology and gravity data (Roddaz et al., 2005b) or in the Beni-Madre de Dios basin to the south, testified by a river gradient change (Aalto et al., 2003) or simply highlighted by structural and geomorphic cross-sections (Baby et al., 1999; Roddaz et al., 2006). The forebulge has been traced up to southern Bolivia (Horton and DeCelles, 1997). The time evolution of the behaviour of a forebulge is difficult to assess because it may have changed both in terms of magnitude and position when subduction velocity, Andes topography or foreland basin filling varied (see Garcia-Castellanos, 2002; see Catuneanu, 2004).

3 Data and methods

We studied the entire Fitzcarrald highlands, which lie between latitudes 6°S and 13°S and longitudes 67°W and 75°W (Fig. 3). We used the free Shuttle Radar Topography Mission (SRTM) Digital Elevation Model (DEM), with a pixel size of 90 m and an absolute vertical accuracy better than 10 m (Farr et al., 2007). Actually, recently published data indicates that the Amazonian forest canopy must offset the signal for about 20 m, as the sensor "sees" the tree tops rather than the earth surface itself (Berry et al., 2007)(cf. Appendix A).

Data were processed with TAS freeware (Terrain Analysis System; Lindsay, 2005). River networks were extracted and classified according to Strahler's method (1952). A total of 2207 5^{th}-order and 90 7^{th}-order catchments were extracted. The 5^{th}-order ones represent a "local" signal (at the Amazon Basin scale; they cover 134 km^2 on average), whereas the 7^{th}-order ones represent the major catchment scale (3660 km^2 on average). Moreover 5^{th}-order and 7^{th}-order catchments allow one to distinguish between two kinds of catchments: the 7^{th}-order ones correspond to the main river drainage areas, whereas 5^{th}-order ones correspond to their tributaries. For these catchments the following values are calculated: *hypsometric integral*, *surface*, *elongation* and *azimuth*. They will allow recognition of the relative maturity of the catchments and river networks. Indeed we assume that when the Arch relief began to form, the river network (and consequently catchment's design) progressively appeared following river erosion. After appearance, internal rearrangements changed the initial morphology that allows us to discriminate young catchments/networks from older or more mature ones. Defining the main trends in the maturity indicators is the aim of this study.

The *hypsometry* is the distribution of elevations in a catchment. The hypsometric curve is its distribution function; after being standardized by scaling elevation and area by the maximum values it can be integrated to obtain the *hypsometric normalised integral* (*H*), given in percent (Strahler, 1952). Hypsometry has classically been used in fluvial landscapes to

212 differentiate erosional landforms at progressive stages in their evolution (Strahler, 1952;
213 Schumm, 1956): the lower *H* is, the more mature is the network (i.e., the older it is). Later
214 works have indicated that the *H*-value may be equivocal. In particular, it has been shown to be
215 dependant on climate, lithology, tectonics, catchment area or sediment transport parameters
216 (Lifton and Chase, 1992; Willgoose and Hancock, 1998; Hurtrez et al., 1999b; Chen et al.,
217 2003; e.g., Brocklehurst and Whipple, 2004). The study area is homogeneous in terms of
218 climate and sediment transport, there are few lithological variations and tectonics are absent
219 except in the Moa Divisor in the northern part. The catchments we compare have the same
220 Strahler order that prevents any inference from variations in catchment areas. All this allows
221 the use of the hypsometric integral in estimating the relative maturity of the catchments.
222 However, such an indicator is of moderate confidence: that is why its distribution over the
223 study area will be discussed together with the elongation parameter for two catchment sizes.

224 In the densely forested study area, hypsometry may exhibit some other errors due
225 either to canopy effect or sedimentation zones. First, canopy affects hypsometry as it offsets
226 the apparent elevation by about 20 m (Berry et al., 2007). The offset of an entire catchment
227 has no effect on its hypsometric integral. In turn, the offset of a forest catchment leading to a
228 major river whose elevation is not offset because it is not forested, can affect significantly the
229 hypsometric integral value. Our calculations (see Appendix A) indicate that for intermediate
230 *H*-values (40-60%), a correction of more than 10 points is required for catchment relief
231 (difference between the highest and lowest catchment elevation) below 100-140 m. Therefore
232 we regard the canopy effect as critical when catchment relief is less than 100 m. Second,
233 depositional areas are likely to alter the observed signal. Observation of the Fitzcarrald Arch
234 topography indicates dendritic and radial drainage catchments typical of erosion-driven
235 geomorphology. Only small and well-defined areas are depositional, they are the Madre de
236 Dios basin to the south-east, the Ucayali basin to the north-west and the Jurua valley

(Figs. 2, 6). This allows us to consider that this effect is of minor influence in the study area. One can note that outside our study area, the Amazon Basin displays catchments with very low relief and with areas where deposition occurs, like the northern and southern Amazonian foreland basins (Fig. 1); hence studying hypsometry there would suffer much more uncertainties.

Elongation (*E*) is the ratio between the diameter of a circle with a surface equal to that of the catchment (*S*, in km^2) and catchment length (*L*): $E = 2\sqrt{(S/\pi)} / L$ (Schumm, 1956; Selby, 1985). *E*-values range between 0 and 1. For circular catchments, *E~1*, for highly elongated catchments, *E<<1*. *E* is close to the number known as the aspect ratio by some authors, which is defined as the ratio between the short and long axis of the catchment (Hurtrez et al., 1999a). This value has two interpretations. First, in active mountain belts, it has been recognised as representative of the slope, and linked to the catchment spacing (Hovius, 1996; Hurtrez et al., 1999a). This definition appears related to still developing drainage networks. On the contrary, for developed networks, the tendency is that various processes, like stream capture, increase catchment width and hence *E* tends to increase (Hancock and Willgoose, 2001). Low *E*-values indicate catchments of high relief due to structural or other controls (e.g., Suresh, 2000; e.g., Solyom and Tucker, 2007). After Willemin and Knuepfer (1994), high *E* indicates the "relative dominance of erosion and processes of catchment integration over uplift". In other words, mature catchments have high *E*, immature catchments have low *E*.

Azimuth (*A*) is the catchment drainage direction, in degrees clockwise from the north. It can be calculated for solely catchments but a local average azimuth *Al* has been calculated which corresponds to averaging the 5th-order catchment azimuths over 80 km x 80 km square cells.

The Fitzcarrald Arch is ideally located for this analysis since the different parts of the Amazon Basin to the north, east, and south lie at low elevations of the order of 100 to 200 m (Fig. 2). Consequently, none of the properties we look at are affected by spatial variations of the base level. In the following, data are presented on maps, and discussion focuses on the Arch's spatial organisation regarding each specific property.

4 Results

4.1 Hypsometry

7^{th}-order catchment hypsometric integrals *H* range from 10% to 68% (Fig. 6a): they qualitatively be grouped into classes of relatively low (less than 30%), intermediate (30%-45%) and high *H*-values (higher than 45%). Low *H*-values (values between 10 and 25%) are found to the north-west, around the Moa Divisor range. Low to intermediate values (15%-35%) are also present to the south-west, at the boundary between the Fitzcarrald Arch and the Subandean zone, where some catchments cross the Subandean Thrust Front. The central part of the Fitzcarrald Arch is characterized by relatively intermediate to high hypsometric integrals (between 40 and 50%), and higher *H*-values at its north-eastern and eastern boundaries (more than 50%, up to 65%, Fig. 6a).

Because of their size, 7^{th}-order catchments are not greatly affected by the errors that could alter the hypsometric signal. On the contrary, the 5^{th}-order catchments could be affected by such errors. Consequently, In spite of a greater spatial accuracy, 5^{th}-order catchments hypsometric integral *H* map is less informative than expected (Fig. 6b). Nevertheless it shows the same pattern than the 7^{th}-order catchments *H* map (Fig. 6a). Moderate hypsometric integrals characterize the centre of the Arch. Areas of lower values characterize the north-western part of the Arch, in the Moa Divisor and to the south, nearby the Subandean front (Fig. 6b). Higher values lie to the NE and to the SE.

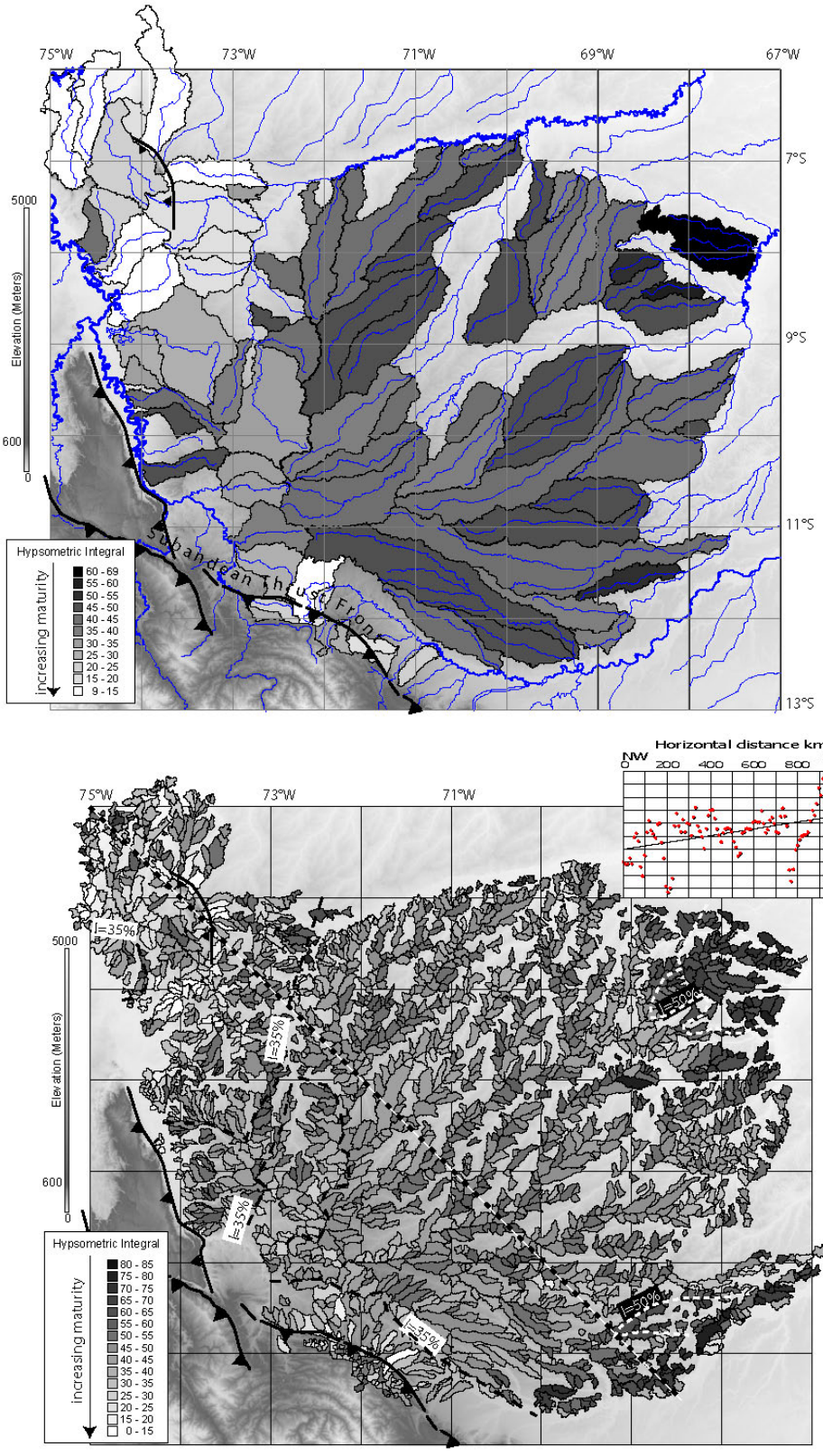

Figure 6. *Fitzcarrald Arch catchments' hypsometric integrals H (in percent), with 7th-order catchments' hypsometric integral contours for H=35% and H=50% . (a) 7th-order catchments, with main tectonic features; (b) 5th-order catchments. Dotted line is a cross*

section shown in top right inset, with regression line. For technical reasons, the section was realised on a best fitting surface of the 5th-order catchments H-value.

4.2 Elongations

7th-order catchments elongation *E*-values are shown in Fig. 7. They range from 0.33 to 0.88. Relatively high *E*-values are found in the north-western part (0.42 to 0.78) and in the south-western part of the Arch, near the subandean zone (0.50 to 0.85). Relatively low *E*-values are found to the south-east (from 0.33 to 0.66) and one at 0.81 in the Madre de Dios Basin (Fig. 7). Intermediate *E*-values are found near the Arch centre and to the north-east (0.42-0.88), areas where high values are found in low-elevation areas. 5th order catchment analysis gives the same kind of result but it is more noisy.

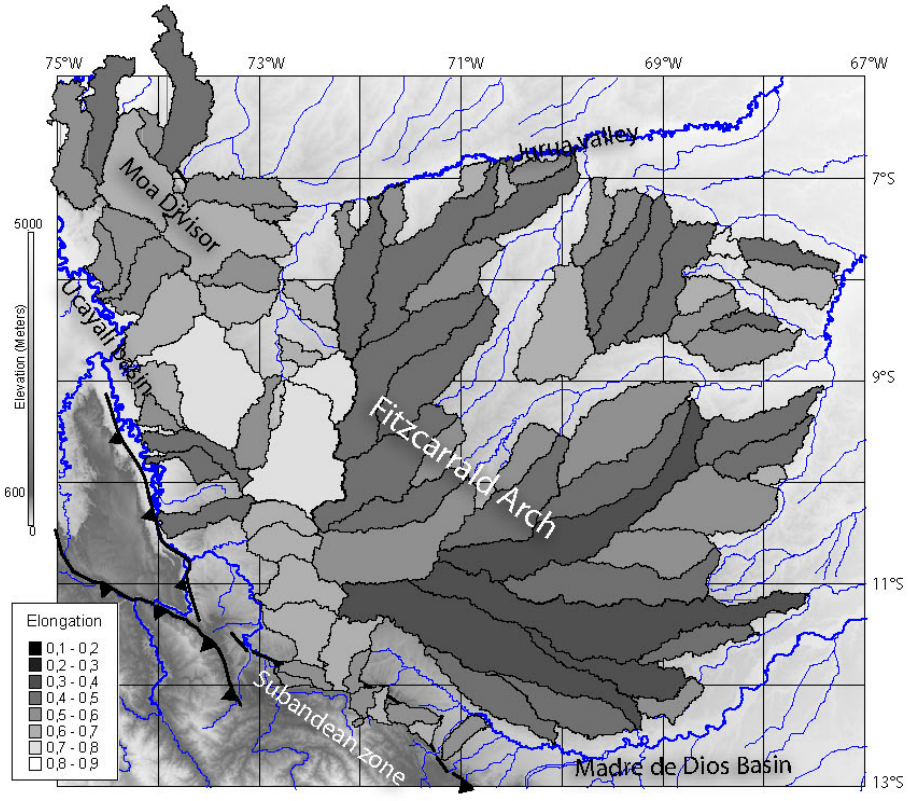

Figure 7. *Fitzcarrald Arch 7th-order catchments' elongation E-value. Note the scale is inverted to represent most mature catchments in light grey and less mature ones in dark grey as for Fig. 6. Note the 72°20'W meridian marks a boundary between a low E-value-domain to the east and a high E-value-domain to the west.*

The Fitzcarrald Arch displays a general trend of decreasing *E*-values from west to south-east. Intermediate *E*-values are found in the north-west (Moa Divisor) and south-west

(Subandean zone). *E*-values around the Arch have a clockwise decreasing trend from west to south-east.

4.3 Azimuths

7th-order catchment azimuths are shown in the Fig. 8. This figure is roughly organized in two parts, east and west of meridian 72°W (Fig. 8). West of this meridian and near the Subandean zone to the south, no obvious catchment organization is recognised. On the contrary the eastern part is radially organised: the azimuths vary clockwise from N0°E to the north to N130°E to the south-east. In the latter, exceptions are found in the north-easternmost part where catchments trend ~N100°E. Note that, catchment azimuth seems more informative when catchments are highly elongated (low *E*-values).

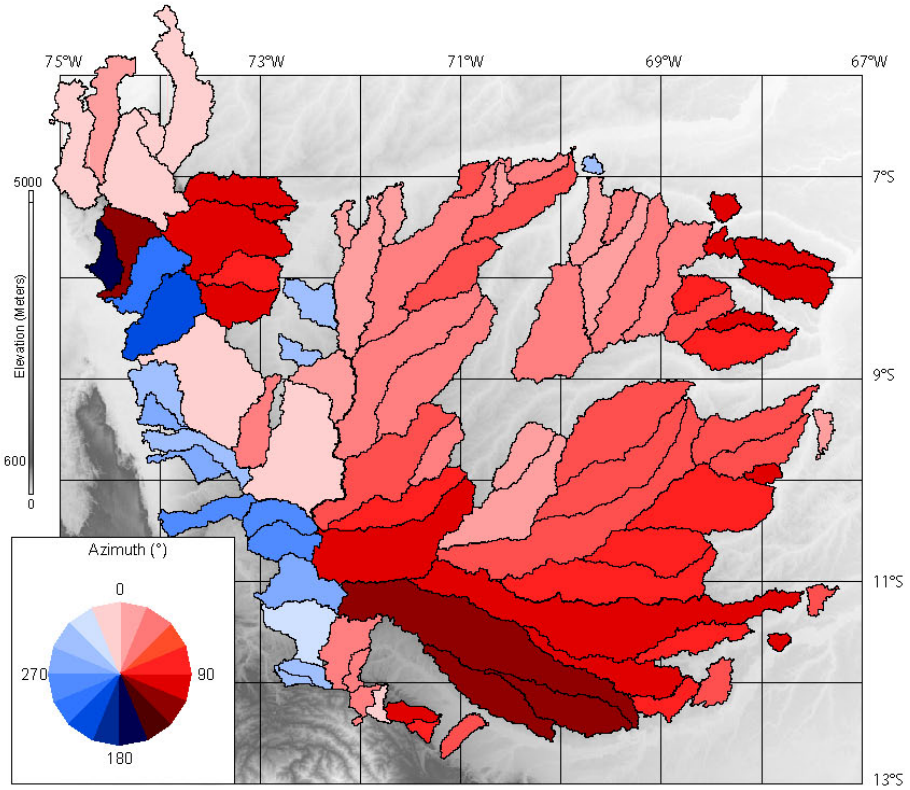

Figure 8. *Fitzcarrald Arch 7th-order catchments' azimuths. The rose indicates Azimuth scale; blue and red colours indicate azimuth west and east, respectively, of a NNW-trending line. Note the 72°20'W meridian seems to separate two distinct domains: no clear organization is found to the west in contrast to the eastern part where the rivers display a clear radial pattern.*

If the picture from 7th-order catchment azimuths (Fig. 8) is informative east of meridian 72°W, the interpretation of the western part is not straightforward. Thus we performed the local average azimuths *Al* for 5th-order catchments to have a more detailed view (Fig. 9). The Arch network appears to radiate from a major 'focal' point; small disturbances seem to be due to three minor 'focal' points. The major 'focal' point is situated at 10.5°S and 72.5°W (denoted by a star in Fig. 9) and may explain the first-order drainage pattern of the Arch. It corresponds to the centre of the radial drainage organisation highlighted in Fig. 8. Superimposed to this large scheme whose wavelength is about 500 km, three second-order 'focal points' or drainage centres (wavelength ~100 km) cause local divergences. Two of them have been previously noticed as particular zones: the Moa Divisor to the north-west, and the Abancay area in the Subandean zone; this last one being discussed even if not really located within the Arch because it disturbs the Arch's drainage organisation (Figs. 6, 7, 9). The third second-order 'focal' point, the Altos de Acre, where catchments diverge towards the Jurua and Purus/Chandlees rivers, is the place we previously noticed as being disturbed from the overall Arch organisation (Figs. 8, 9).

5 Discussion

Both elongations and hypsometric integrals for 5th-order and 7th-order catchments show a relief maturity decrease from north-west at Moa Divisor to the south-east near the Madre de Dios basin and to the north-east (Altos de Acre); the most mature catchments are found to the south-east. A small part to the south-west near by the Subandean zone displays mature catchments.

Drainage azimuth aids the understanding of this scheme. It indicates that there is a first-order relief, which can be called the Fitzcarrald Arch *sensu stricto*, whose centre is situated ~100 km north-east from the Subandean Thrust Front at 10.5°S and 72.5°W, and which covers the entire study area with the exceptions of the Moa Divisor and the Subandean

zone. According to the maturity gradient, from mature in the north-west to immature in the south-east, this relief seems to have formed recently with a north-west to south-east progression, with three exceptions disturbing this simple scheme. These correspond to the three minor 'focal' points described before: the Altos de Acre, the Moa Divisor and the Subandean zone.

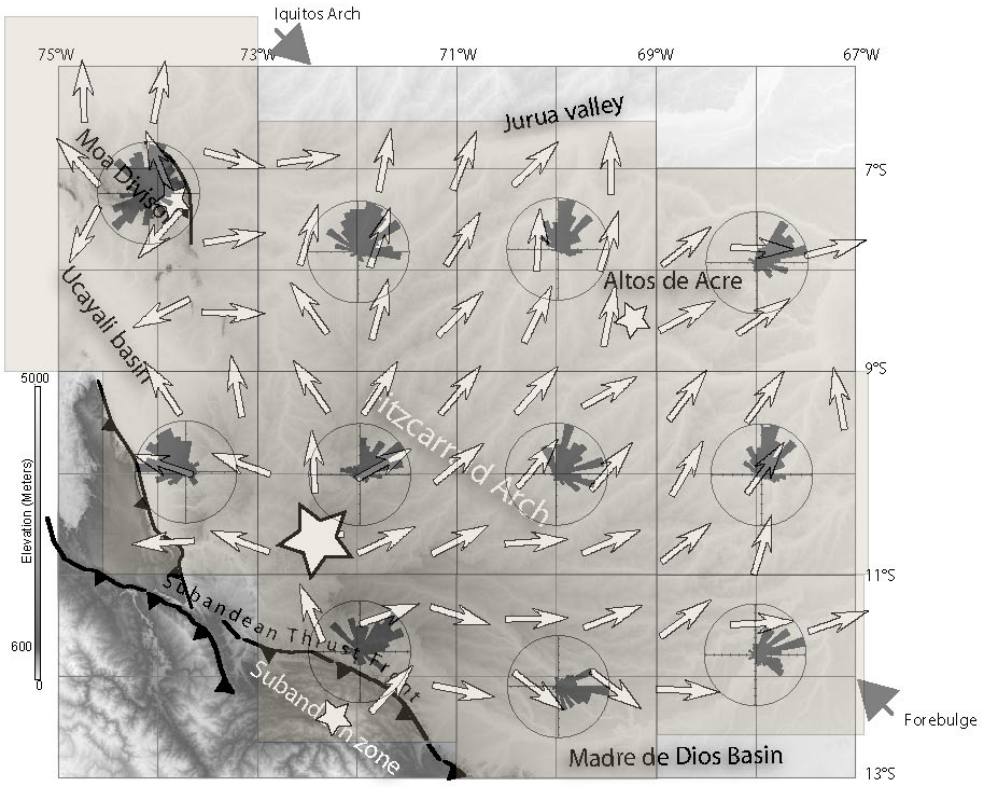

Figure 9. *Fitzcarrald Arch 5th-order catchments' locally averaged azimuths (arrows); roses for approximately 2 x 2 sq. degrees (rectangles) are indicated. Big star represents the approximate location for Fitzcarrald Arch divergent drainage centre ('focal' point). Small stars represent local centres for diverging drainages that disturb the Fitzcarrald drainage shape. The forebulge axis is shown; to the south-east, after Aalto et al. (2003), to the north-east after Roddaz et al. (2005a) and Dumont et al. (1991).*

The main part of the Arch (without the areas affected by the minor 'focal' points) is first characterized by a clear difference between its eastern and western parts, the boundary between the two being approximately located at longitude 72°20W. The western slope is greater than the eastern one. To the west, catchments have hypsometric integrals between 20% and 65% and 20% and 50% for 5th- and 7th-order catchments, respectively. *E*-values are

between 0.4 and 0.8. To the east, 7th-order catchment hypsometric integrals are distributed around 45% (they are mostly between 35 and 50%) without any clear trend, in contrast to the 5th-order ones which display a clear progression from low values in the north (mostly between 15% and 55%) to high values in the south-east (mostly between 40% and 75%). The 7th-order catchments *E*-values distribution exhibits the same trend, with the lowest values (between 0.3 and 0.4) concentrated in the south-easternmost area. The radial organisation originating at the main 'focal' point is clearer than in the eastern side.

The Altos de Acre minor 'focal' occurs to the north-east. It is characterized by high hypsometric integrals, up to 60%, observed both for 7th- and 5th-order catchments. In particular, with the south-easternmost part of the Arch it shows the highest 5th-order catchments hypsometric integrals. *E*-values are relatively low but not as low as they stand elsewhere in the Arch. *E*-values and hypsometry indicates that the relief in the area may have formed recently; the fact the catchments (both 5th- and 7th-order ones) are not so elongated (not so low *E*-values), could indicate an older set-up, that is to say the current stage is an accentuation or rejuvenation of the relief with a low degree of drainage reorganisation. Its cause is unclear; it could be an expression of the forebulge which was found at the Iquitos Arch more to the north (Roddaz et al., 2005b) or in the Madre de Dios basin to the south (Aalto et al., 2003; Roddaz et al., 2006). The Altos de Acre is interestingly located in between and we speculate it could be the subtle topographic expression of the forebulge. It is difficult to go further in terms of explanation as the forebulge could have moved with the rise of the Arch and also because the dip of the subduction is likely to have changed the dynamic topography (here also with little constraints on the location and magnitude of the phenomenon, e.g., Dávila and Lithgow-Bertelloni, 2008).

The Moa Divisor displays the lowest hypsometric integrals and particularly high *E*-values, both for 5th- and 7th-order catchments. Thus, it appears to be an important relief, older

than the other parts of the Arch. Regarding the drainage directions, clearly differing from the Fitzcarrald Arch, it apparently evolved independently. This is probably due to the thrust activity underneath (Mégard, 1984) as shown by seismic profiles in its northern edge (Hermoza et al., 2005; Hermoza et al., 2006).

The Subandean zone catchments have low hypsometric integrals: lower than 45% and 35% for the 5^{th}- and 7^{th}-order ones, respectively; and they are not significantly elongated (*E*-values around 0.6). Moreover and contrary to that expected, the Subandean Thrust Front does not significantly affect the Fitzcarrald Arch drainage organisation. This argues for little recent relief development. This does not support the particular role ascribed by some authors to the intriguing Abancay structure in actual drainage pattern and evolution (Marocco, 1978). On the contrary, our observation confirms the conclusions of others (Arriagada et al., 2006; Roperch et al., 2006; Carlotto et al., 2007), which indicate that this structure exhibits no or little activity in recent times (since the Miocene).

The most important result of our study is the clear progression from old to young catchments from north-west to south-east, with a Subandean zone not significantly generating relief. It is difficult to date the initiation of these catchments and their relief; and the results presented here are valuable as they lead at least to a relative chronology for the catchments. Interestingly, this migration of the relief generation location is similar to the reconstruction by Hampel (2002), implying a sliding from NW to SE of the Nazca ridge under the South American plate. Meanwhile, our observations do not agree with the possibility of an alluvial fan. First, the Fitzcarrald main drainage network centre is not located at a major catchment outlet like it should be if it corresponded to a fan but is relatively far from the Andean catchment outlets in the Amazon Basin. And a third argument against the fan is provided by the seismic lines (Fig. 5 and Espurt, 2007) on which Mesozoic strata show an uplift roughly parallel to the current topography, very different from the characteristic sediment

417 accumulation of (mega)fans from which the Fitzcarrald Arc is also different by its
418 characteristic slopes (up to 0.3° whereas south Bolivian Subandean fans exhibit slopes of
419 ~0.05°, Horton and DeCelles, 2001).

420 The Fitzcarrald Arch formation is not more likely the result of any motion along the
421 Pisco–Abancay–Fitzcarrald lineament, which would imply an anticline structure elongated in
422 a NE-SW direction, different from our radial structure (Fig. 3). Moreover, no reactivated
423 structure under the expected transfer zone can be seen on seismic profiles (Fig. 4) (Espurt,
424 2007). Thus, our study results favour the scenario of initial subduction and sliding of the
425 Nazca Ridge from WNW to ESE pushing up the South American lithosphere, originating the
426 Arch's dome-like structure.

427 This hypothesis of surface uplift due to the sliding of the Nazca Ridge beneath the
428 South America lithosphere is moreover supported by other observations. First, the underlying
429 subducted Nazca Ridge length should increase when sliding from north-west to south-east
430 since 5 My (Hampel, 2002). Consequently, its effect was initially slight and increased to the
431 present, and the northern catchments became progressively enlarged: it may also be
432 responsible for the intermediate maturity catchments found in the centre and the north of the
433 Fitzcarrald Arch. Second, as shown by Espurt et al. (2007), the lithologic formations do not
434 show important thickness variations, and the relief appears more likely related to a crustal
435 doming, incompatible with a crustal thickening, than due to huge sediment supply necessary
436 for fan building. Subsurface data presented by Espurt et al. (2007) show that the Fitzcarrald
437 Arch regional uplift incorporates deep-seated Palaeozoic structures. These structures are NE-
438 trending and are not reactivated. In contrast, the northern Moa Divisor shows typical N-
439 trending thick-skinned structures. The subduction of the Nazca ridge may have controlled the
440 reactivation of the Moa Divisor Paleozoic structure probably before the uplift of the
441 Fitzcarrald Arch. Thus, the horizontal stress-induced by the SE-migration of the Nazca ridge

beneath the South American plate seems to have reactivated N-trending thrusts, whereas oblique, NE-trending structures are still sealed by Cretaceous strata (Espurt et al., 2007). The Moa Divisor structure may be interpreted as the Peruvian equivalent of the thick-skinned thrusts of the Sierras Pampeanas above the Central Chile/NW Argentina flat slab (Jordan et al., 1983).

Larger scale observation shows this Arch is bounded by two major foreland catchments (foredeeps, Fig. 1), the northern Amazonian foreland basin (or Marañon-Ucayali basin) and the southern Amazonian foreland basin (or Beni-Mamore basin) to the south. Further research should investigate the relationships between a Fitzcarrald Arch-like structure and these basins.

6 Conclusions

The Fitzcarrald Arch constitutes a wide relief within the Amazon Basin, located nearby the central Andes. We produced a quantitative study of the drainage catchments located in the area, exploring hypsometry, elongation and azimuth directions of both Strahler 5^{th}- and 7^{th}-order catchments. The data clearly indicate a general decrease in the catchment maturity from north-west to south-east, interpreted as evidence for lower ages for catchments and river networks becoming established to the south-east. Second order features are also highlighted: the Moa Divisor being a young thrust, the Subandean Zone slightly affecting the Amazonian lowlands relief, and the Altos de Acre being related to the forebulge of the Amazonian foreland basin.

The Fitzcarrald arch cannot represent one of the widest alluvial fans in the world, since its apex is badly located (100 km east to the Subandean Thrust Front) and since the corresponding sedimentary pile is lacking. Nor can it be the superficial expression of an inherited transfer zone since its geomorphic organization is radial and does not diverge from an axis; in addition such a reactivated structure is not found at depth in seismic profiles.

Conversely, our data show the underlying geomorphic control has progressed from NW to SE, which with the observation of crustal doming by Espurt et al. (2007) suggest that this relief is caused by the eastward sliding of the buoyant Nazca ridge segment under the South American lithosphere. Consequently, the recent uplift of the Fitzcarrald Arch is younger than 1) the uplift of the Moa Divisor range related to Andean compression, and 2) the development of the late Miocene Iquitos forebulge linked to the elastic component of the South America plate (Roddaz et al., 2005a). If this explanation is correct, the Fitzcarrald Arch is an impressive example of relief development with neither shortening nor any active tectonics being expressed.

We propose that this recent relief is due to the buoyancy and coupling between the two plates. N-trending reactivated Palaeozoic structures are observed in the Amazonian foreland basin but they are localized to the north of the Fitzcarrald Arch uplift. This setting can be compared with the Sierras Pampeanas (Argentina) where the Juan Fernandez Ridge flat subduction led to the inversion of old structures. Interestingly, seismic data on the Fitzcarrald Arch show NE-trending Palaeozoic structures incorporated in the regional bulge. These structures are non-reactivated and sealed by Cretaceous strata (Espurt et al., 2007). We suggest that the absence of tectonic activity in the Fitzcarrald Arch area may result from the incompatibility of the NE-trending structure with reactivation.

7 Acknowledgements

We wish to thank ECLIPSE and RELIEF programs for financial support, and the IRD-PERUPETRO S.A. research agreement. This work results from interesting discussions with J. Martinod, D. Chardon and S. Carretier. Two anonymous reviewers and Editor A. Plater offered criticism for manuscript improvement.

8 Appendix: Canopy effect

A first order canopy effect is that corresponding to a drop of ~20 m at the catchment outlet. In terms of hypsometry its effects can be evaluated by removing a strip equivalent to ~20 m in the bottom of hypsometry (Fig. A). Hence the corrected hypsometric integral is *I'* in percent, catchment relief *R* in meters and canopy effect *C* in meters.

$$I' = \left(I - \frac{C}{R} \times 100\right) \cdot \frac{I}{I-R}$$

His correction appears relevant, since most of the time when made, it permits recovery of the main trend of hypsometries in the area, as illustrated by 5th-order catchments form the Alto Jurua Area (Figs. 2, 6b, A).

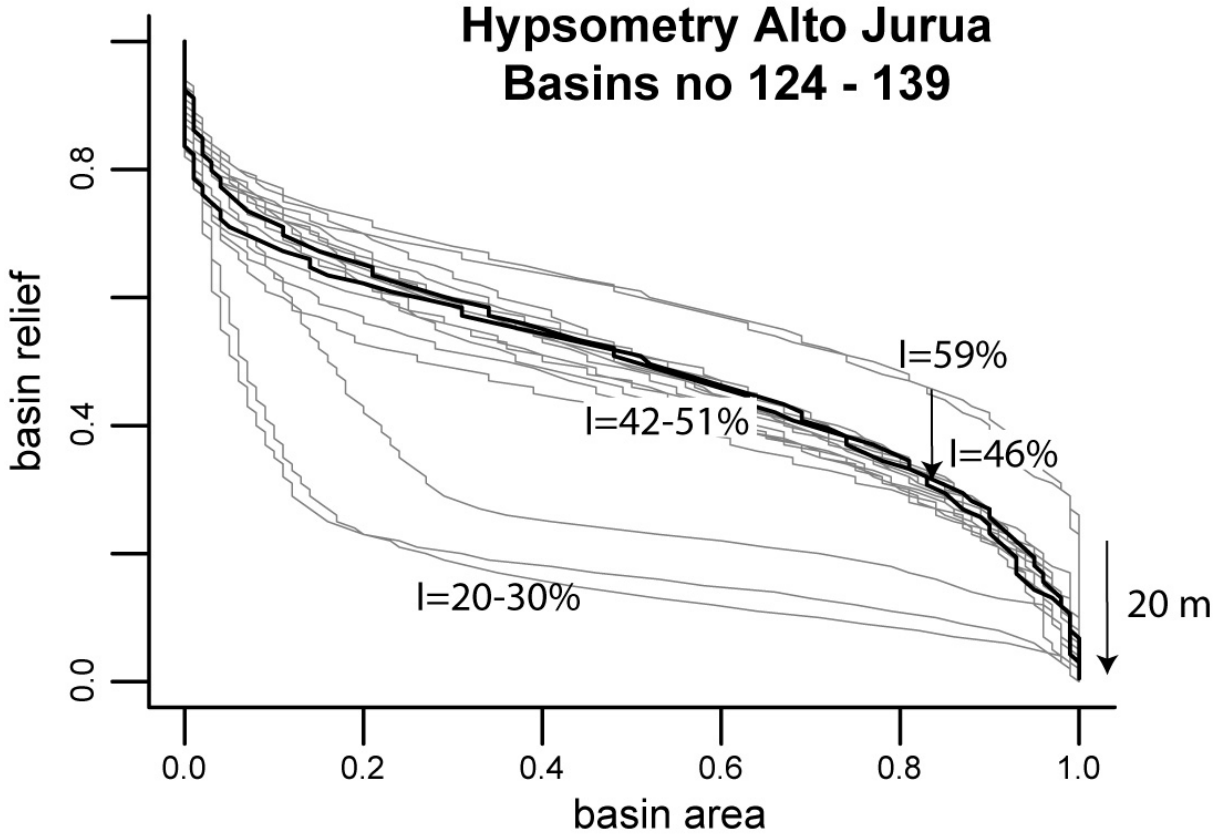

Figure A. Canopy effect, example from Alto Jurua 5th-order catchments n# 124 to 139. Catchment hypsometric integrals *H* evaluated from SRTM are in grey. Catchments n# 134 and 138 which display a step at their bottom (original relief ~85m) have been corrected for canopy, in black. Most of the catchments have an apparent hypsometric integral ranging from 42 to 51%; three have low integral of 20 to 30%; and the two with a step are about 59%, but this value decreases to 46% when corrected for canopy, thus corresponding to the main trend.

9 References

Aalto, R., Maurice-Bourgoin, L., Dunne, T., Montgomery, D.R., Nittrouer, C.A., Guyot, J.L., 2003. Episodic sediment accumulation on Amazonian flood plains influenced by El Niño/Southern Oscillation. Nature, 425, 493-497.

Arriagada, C., Cobbold, P.R., Roperch, P., 2006. Salar de Atacama basin: A record of compressional tectonics in the central Andes since the mid-Cretaceous. Tectonics, 25, TC1008.

Baby, P., Guyot, J.-L., Deniaud, Y., Zubieta, D., Christophoul, F., Rivadeneira, M., 1999. The High Amazonian Basin: Tectonic control and mass balance, in HyBAm (Hydrology and geochemistry of the Amazon BAsin), Hydrological and Geochemical Process in Large-Scale River, Manaus.

Berry, P.A.M., Garlick, J.D., Smith, R.G., 2007. Near-global validation of the SRTM DEM using satellite radar altimetry. Remote Sensing Of Environment, 106, 17-27.

Brocklehurst, S.H., Whipple, K.X., 2004. Hypsometry of glaciated landscapes. Earth Surface Processes And Landforms, 29, 907-926.

Carlotto, V., Cárdenas, J., Tintaya, D., Rodríguez, R., Valdivia, W., 2007. Altos estructurales en el control de la evolucion andina: la deflexion de Abancay y el Arco de Manu, XIII Congreso Peruano de Geología. Sociedad Geológica del Perú, Lima, pp. 248.

Catuneanu, O., 2004. Retroarc foreland systems - evolution through time. Journal Of African Earth Sciences, 38, 225-242.

Chen, Y.-C., Sung, Q., Cheng, K.-Y., 2003. Along-strike variations of morphotectonic features in the Western Foothills of Taiwan: tectonic implications based on stream-gradient and hypsometric analysis. Geomorphology, 56, 109-137.

Christophoul, F., Baby, P., Soula, J.-C., Rosero, M., Burgos, J., 2002. Les ensembles fluviatiles neogenes du bassin subandin d'Equateur et implications dynamiquesThe Neogene fluvial systems of the Ecuadorian foreland basin and dynamic inferences. Comptes Rendus Geosciences, 334, 1029.

Church, G.E., 1901. South America: An Outline of Its Physical Geography. The Geographical Journal, 17, 333-406.

Daly, D.C., Mitchell, J.D., 2000. Lowland vegetation of tropical South America -- an overview. In: D. Lentz (Editor), Imperfect Balance: Landscape Transformations in the pre-Columbian Americas. Columbia University Press, New York, pp. 391-454.

Dávila, F.M., Lithgow-Bertelloni, C., 2008. Dynamic topography during flat-slab subduction: A first approach in the south-Central Andes, 7th International Symposium on Andean Geodynamics (ISAG 2008), Nice, pp. 176-179.

DeMets, C., Gordon, R.G., Argus, D.F., Stein, S., 1990. Current Plate Motions. Geoph. J. Int., 101, 425-478.

Dumont, J.F., 1996. Neotectonics of the Subandes-Brazilian craton boundary using geomorphological data: the Maranon and Beni basins. Tectonophysics, 259, 137.

Dumont, J.F., Deza, E., Garcia, F., 1991. Morphostructural provinces and neotectonics in the Amazonian lowlands of Peru. Journal of South Americal Earth Sciences., 4, 373-381.

Espurt, N., 2007. Influence de la subduction d'une ride asismique sur la dynamique de la plaque continentale chevauchante: exemple de la ride de Nazca et du bassin amazonien. PhD Thesis, University of Toulouse, Toulouse.

Espurt, N., Baby, P., Brusset, S., Roddaz, M., Hermoza, W., Barbarand, J., submitted. The Nazca Ridge and uplift of the Fitzcarrald Arch: Implications for regional geology in northern South America, Amazonian, Landscape and Species Evolution: A Look into the Past. Blackwell.

555 Espurt, N., Baby, P., Brusset, S., Roddaz, M., Hermoza, W., Regard, V., Antoine, P.O., Salas-
556 Gismondi, R., Bolaños, R., 2007. How does the Nazca Ridge subduction influence the
557 modern Amazonian foreland basin? Geology, 35, 515-518.
558 Espurt, N., Brusset, S., Baby, P., Hermoza, W., Bolanos, R., Uyen, D., Deramond, J., 2008a.
559 Paleozoic structural controls on shortening transfer in the Subandean foreland thrust
560 system, Ene and southern Ucayali basins, Peru. Tectonics, 27, TC3009, DOI:
561 10.1029/2007TC002238.
562 Espurt, N., Funiciello, F., Martinod, J., Guillaume, B., Regard, V., Faccenna, C., Brusset, S.,
563 2008b. Flat subduction dynamics and deformation of the South American plate:
564 Insights from analog modeling. Tectonics, 27, TC3011, DOI:
565 10.1029/2007TC002175.
566 Farr, T.G., Rosen, P.A., Caro, E., Crippen, R., Duren, R., Hensley, S., Kobrick, M., Paller,
567 M., Rodriguez, E., Roth, L., Seal, D., Shaffer, S., Shimada, J., Umland, J., Werner,
568 M., Oskin, M., Burbank, D., Alsdorf, D., 2007. The Shuttle Radar Topography
569 Mission. Rev. Geophys., 45, RG2004, doi:10.1029/2005RG000183.
570 Garcia-Castellanos, D., 2002. Interplay between lithospheric flexure and river transport in
571 foreland basins. Basin Research, 14, 89-104.
572 Gingras, M.K., Rasanen, M.E., Pemberton, S.G., Romero, L.P., 2002. Ichnology and
573 sedimentology reveal depositional characteristics of bay-margin parasequences in the
574 Miocene Amazonian foreland basin. Journal of Sedimentary Research, 72, 871-883.
575 Gutscher, M.A., 2002. Andean subduction styles and their effect on thermal structure and
576 interplate coupling. Journal of South American Earth Sciences, 15, 3-10.
577 Gutscher, M.A., Olivet, J.L., Aslanian, D., Eissen, J.P., Maury, R., 1999. The "Lost Inca
578 Plateau": cause of flat subduction beneath Peru? Earth and Planetary Science Letters,
579 171, 335-341.
580 Gutscher, M.A., Spakman, W., Bijwaard, H., Engdahl, E.R., 2000. Geodynamics of flat
581 subduction: Seismicity and tomographic constraints from the Andean margin.
582 Tectonics, 19, 814-833.
583 Hampel, A., 2002. The migration history of the Nazca Ridge along the Peruvian active
584 margin: a re-evaluation. Earth and Planetary Science Letters, 203, 665-679.
585 Hancock, G., Willgoose, G., 2001. Use of a landscape simulator in the validation of the
586 SIBERIA catchment evolution model: Declining equilibrium landforms. Water
587 Resources Research, 37, 1981-1992.
588 Hermoza, W., Baby, P., Espurt, N., Martinez, E., Bolaños, R., 2006. Lateral variations in the
589 Subandean deformation of the Ucayali basin: a complex fold-thrust belt and inverted
590 basin, XIII Congreso Peruano de Geología, Lima.
591 Hermoza, W., Brusset, S., Baby, P., Gil, W., Roddaz, M., Guerrero, N., Bolanos, R., 2005.
592 The Huallaga foreland basin evolution: Thrust propagation in a deltaic environment,
593 northern Peruvian Andes. Journal of South American Earth Sciences, 19, 21.
594 Horton, B.K., DeCelles, P.G., 1997. The modern foreland basin system adjacent to the Central
595 Andes. Geology, 25, 895-898.
596 Horton, B.K., DeCelles, P.G., 2001. Modern and ancient fluvial megafans in the foreland
597 basin system of the central Andes, southern Bolivia: implications for drainage network
598 evolution in fold-thrust belts. Basin Research, 13, 43-63.
599 Hovikoski, J., Gingras, M., nen, M., Rebata, L.A., Guerrero, J., Ranzi, A., Melo, J., Romero,
600 L., del Prado, H.N., ez, Jaimes, F., Lopez, S., 2007. The nature of Miocene
601 Amazonian epicontinental embayment: High-frequency shifts of the low-gradient
602 coastline. Geological Society of America Bulletin, 119, 1506-1520.

603 Hovikoski, J., Rasanen, M., Gingras, M., Roddaz, M., Brusset, S., Hermoza, W., Pittman,
604 L.R., 2005. Miocene semidiurnal tidal rhythmites in Madre de dios, Peru. Geology,
605 33, 177-180.
606 Hovius, N., 1996. Regular spacing of drainage outlets from linear mountain belts. Basin
607 Research, 8, 29-44.
608 Hurtrez, J.-E., Lucazeau, F., Lavé, J., Avouac, J.-P., 1999a. Investigation of the relationships
609 between basin morphology, tectonic uplift, and denudation from the study of an active
610 fold belt in the Siwalik Hills, central Nepal. J. Geophys. Res., 104, 12,779-12,796.
611 Hurtrez, J.E., Sol, C., Lucazeau, F., 1999b. Effect of drainage area on hypsometry from an
612 analysis of small-scale drainage basins in the Siwalik Hills (Central Nepal). Earth
613 Surface Processes And Landforms, 24, 799-808.
614 Jacques, J., 2003. A tectonostratigraphic synthesis of the Sub-Andean basins: implications for
615 the geotectonic segmentation of the Andean Belt. Journal of the Geological Society,
616 160, 687.
617 Jordan, T.E., Isacks, B.L., Allmendinger, R.W., Brewer, J.A., Ramos, V.A., Ando, C.J., 1983.
618 Andean tectonics related to geometry of subducted Nazca plate. Geol. Soc. Am. Bull.,
619 94, 341-361.
620 Kronberg, B.I., Fralick, P.W., Benchimol, R.E., 1998. Late Quaternary sedimentation and
621 palaeohydrology in the Acre foreland basin, SW Amazonia. Basin Research, 10, 311-
622 323.
623 Latrubesse, E.M., Rancy, A., 2000. Neotectonic influence on tropical rivers of southwestern
624 Amazon during the late quaternary: the Moa and Ipixuna river basins, Brazil.
625 Quaternary International, 72, 67-72.
626 Lifton, N.A., Chase, C.G., 1992. Tectonic, climatic and lithologic influences on landscape
627 fractal dimension and hypsometry: implications for landscape evolution in the San
628 Gabriel Mountains, California. Geomorphology, 5, 77-114.
629 Lindsay, J.B., 2005. The Terrain Analysis System: A tool for hydro-geomorphic applications.
630 Hydrological Processes, 19, 1123-1130.
631 Marocco, R., 1978. Un segment E-W de la chaîne des Andes péruviennes: La déflexion
632 d'Abancay. Etude géologique de la Cordillère Orientale et des hauts plateaux entre
633 Cuzco et San Miguel. Travaux et Documents de l'ORSTOM. ORSTOM, 195 pp.
634 Mégard, F., 1984. The Andean orogenic period and its major structures in central and
635 northern Peru. Journal of the Geological Society of London, 141, 893-900.
636 Räsänen, M.E., Linna, A.M., Santos, J.C.R., Negri, F.R., 1995. Late Miocene tidal deposits in
637 the Amazonian foreland basin. Science, 269, 386-390, doi:
638 10.1126/science.269.5222.386.
639 Rebata, H.L.A., Rasanen, M.E., Gingras, M.K., Vieira, V., Barberi, M., Irion, G., 2006.
640 Sedimentology and ichnology of tide-influenced Late Miocene successions in western
641 Amazonia: The gradational transition between the Pebas and Nauta formations.
642 Journal of South American Earth Sciences, 21, 96-119.
643 Roddaz, M., Baby, P., Brusset, S., Hermoza, W., Darrozes, J.M., 2005a. Forebulge dynamics
644 and environmental control in Western Amazonia: The case study of the Arch of
645 Iquitos (Peru). Tectonophysics, 399, 87.
646 Roddaz, M., Brusset, S., Baby, P., Herail, G., 2006. Miocene tidal-influenced sedimentation
647 to continental Pliocene sedimentation in the forebulge-backbulge depozones of the
648 Beni-Mamore foreland Basin (northern Bolivia). Journal of South American Earth
649 Sciences, 20, 351-368.
650 Roddaz, M., Viers, J., Brusset, S., Baby, P., Herail, G., 2005b. Sediment provenances and
651 drainage evolution of the Neogene Amazonian foreland basin. Earth and Planetary
652 Science Letters, 239, 57.

Roperch, P., Sempere, T., Macedo, O., Arriagada, C., Fornari, M., Tapia, C., Garcia, M., Laj, C., 2006. Counterclockwise rotation of late Eocene-Oligocene fore-arc deposits in southern Peru and its significance for oroclinal bending in the central Andes. Tectonics, 25.

Schumm, S.A., 1956. Evolution of drainage systems and slopes in badlands at Perth Amboy, New Jersey. Bull Geol. Soc. Am., 67, 597-646.

Selby, M.J., 1985. Earth's Changing Surface: an Introduction to Geomorphology. Oxford University Press, Oxford, 607 pp.

Solyom, P.B., Tucker, G.E., 2007. The importance of the catchment area-length relationship in governing non-steady state hydrology, optimal junction angles and drainage network pattern. Geomorphology, 88, 84-108.

Strahler, A.N., 1952. Dynamic basis of geomorphology. Geological Society of America Bulletin, 63, 923-938.

Suresh, R., 2000. Soil and Water Conservation Engineering 3rd Ed. Standard Publishers, Delhi.

Willemin, J.H., Knuepfer, P.L.K., 1994. Kinematics of arc-continent collision in the eastern Central Range of Taiwan inferred from geomorphic analysis. J. Geophys. Res., 99, 20267-20280.

Willgoose, G., Hancock, G., 1998. Revisiting the hypsometric curve as an indicator of form and process in transport-limited catchment. Earth Surface Processes And Landforms, 23, 611-623.

Woods, M.T., Okal, E.A., 1994. The Structure of the Nazca Ridge and Sala Y Gomez Seamount Chain From the Dispersion of Rayleigh Waves. Geophysical Journal International, 117, 205-222.

Yañez, G., Cembrano, J., Pardo, M., Ranero, C., Selles, D., 2002. The Challenger-Juan Fernandez-Maipo major tectonic transition of the Nazca-Andean subduction system at 33-34 degrees S: geodynamic evidence and implications. Journal of South American Earth Sciences, 15, 23-38.